This is a previous version of the article published in Applied Clay Science. 2020, 198: 105847. https://doi.org/10.1016/j.clay.2020.105847

ASSESSMENT OF MECHANICAL, THERMAL, MINERAL AND PHYSICALL PROPERTIES OF FIRED CLAY BRICK MADE BY MIXING KAOLINITIC RED CLAY AND PAPER PULP RESIDUES

P. Muñoz[*,a,e)]; V. Letelier[b)]; M.A. Bustamante[c)]; J. Marcos-Ortega[d)]; J.G. Sepúlveda[b)]

a) Facultad de Ingeniería. Universidad Autónoma de Chile, 5 Poniente 1760, Talca, Chile

b) Departamento de Obras Civiles, Universidad de la Frontera, Francisco Salazar 1145, Temuco, Chile.

c) School of Construction Engineering, Universidad Católica del Maule, Talca, Chile

d) Departamento de Ingeniería Civil, Universidad de Alicante, 03080, Alicante, Spain

e) Universidad Internacional de La Rioja, Avda. La Paz, 137, INeS Research Group, Spain

* corresponding author: pmunozv@uautonoma.cl

Abstract

Among the largest producers of waste, the paper industry stands out due to its impact on human health and ecological balance. However, these residues may also contribute to a more environmental friendly brick industry, since the incorporation of fluxing agents may improve the firing process and the induced porosity reduces thermal conductivity of fired bricks. Therefore, this study aims to assess the feasibility of replacing clay with solid paper residue (PPR) from 2.5 to 17.5 % in order to reduce resources depletion and improve brick performance. The original clay was characterized as a non-calcareous red clay with high contents of kaolinite. Several samples were made by extrusion and fired at 900 ºC in accordance with industrial procedures. The addition of PPR led to increase shrinkage from 5 to 10% due to the effect of fluxing oxides which reduced pores volume and enlarged pores size. In addition, the impervious fraction was slightly reduced while the apparent porosity certainly increased (i.e. approx. 17 %) due to the macroscopic pores developed by PPR combustion. This porosity produces lighter bricks (i.e. density decays from 1.76 to 1.39 g dm^{-3}) with lower thermal conductivity (i.e. from 5.53 to 0.41 W m^{-1} K^{-1}) but also reduces compressive strength (i.e. from 11 to 3 MPa) and increases water

absorption (i.e. up to 24 %). Nevertheless, toxicity is below the regulatory limits in all cases and fired bricks are easily adaptable to industrial procedures.

Keywords

Clay brick, kaolin, paper residue, recycling, waste

1. Introduction

Due to the raw materials depletion and the environmental impacts associated with their extraction, the construction industry is continuously searching for new alternative materials which are commonly selected from residues (Muñoz et al., 2014, 2016). In spite of some initiatives may be currently available (e.g. the use of ash in cement production, the incorporation of fired clay bricks residues into road basis, the use of recycled aggregates in concrete, etc.), in general, manufacturers have not taken advantage of the large number of available examples from literature. Added to economic aspects, such as the lack of legislation or marketing issues, among others, one of the reasons might be the fact that most researches have been carried out without taking into account industrial procedures.

From decades, paper and pulp industry (PPI) has become an important source of different residues (e.g. bark residues, waste paper, sludge, black liquors, etc.) which have been successfully tested for manufacturing construction materials, among other uses (Mandeep et al., 2020). On the one hand, toxic effluents must be treated prior to be discharged into water bodies. This process generates large amounts of sludge which has been widely assessed for replacing clay in fired bricks (Kizinievič et al., 2018; Vieira et al., 2016) but also for manufacturing mortars, concrete or geopolymers (Vashistha et al., 2019). In spite of investigations concluded positive effects, industrial scale is certainly hindered since sludge must be previously dried and milled in order to allow its handling, storage and use. Besides, characteristics of sludge highly differ among lot and factories, making it necessary to redo the characterization analysis to each lot received as it was demonstrated by Ribeiro dos Santos et al. (2019). In addition, the excess of fluxing agents have led to excessive shrinkage (i.e. more than 25 %) as it was stated by Asquini et al. (2008).

On the other hand, whereas this sludge shows high heterogeneity, the composition of PPI solid waste is well known and mostly constant. The solid PPI residue is mainly composed by wood fibers which are generated from the rejection of screening and/or washing procedures (Monte et al., 2009). In spite of some factories use this solid residue for energy production, the so generated particulate matter and gaseous emissions (e.g. SO_2, and NO_x, among others) frequently hinder its feasibility.

Despite a large number of researches regarding sludge may be highlighted, literature rarely shows the use of PPI solid waste for replacing natural raw materials. Thus, Sutcu and Akkurt (2009) used solid paper and pulp residues (PPR) mixed with non-calcareous clays. Raw materials were initially dried and grinded. Replacement ratios ranged from 10 to 30 % and samples were made by pressing and fired at 1000 ºC. However, when samples were formed by extrusion, same authors limited up to 20 % the addition of PPR. At this PPR replacement ratio, density, thermal conductivity (TC) and compressive strength (CS) decayed 22, 40 and 80 %, respectively. The main issue was related to water absorption (WA) which was increased from 17 to 32 %. Same authors also showed the effect of firing temperature by increasing it up to 1400 ºC with the aim of producing porous anorthite lightweight ceramics by mixing clay and PPR (Sutcu and Akkurt, 2010). Similar reduction rates were observed at this temperature for CS (i.e. from 42 to 8.6 MPa) and bulk density (i.e. from 2.0 to 1.2 g cm^{-3}). It was concluded that traditional clays produced anorthite and gehlenite at low temperatures due to the addition of alkalis in the clay that fluxed the mixtures. During the firing process, these alkaline-earth elements are decomposed between 600 ºC (i.e. $MgCO_3$) and 900 ºC (CaO_3) to form CaO, MgO, and CO_2 which may be trapped within the fired clay matrix or released from it. Shibib (2015) also corroborated these results by replacing calcium rich clays with PPR from 9 to 50 %. Samples were made by pressing and fired at 900 ºC. As result, the effect of PPR was lower. For instance, CS decreased from 51 (i.e. for control samples) to 30 MPa and 26.5 MPa for 17 and 38 % of replacement.

Based on these findings, this paper aims to serve for increasing current knowledge of the use of PPR for fired clay bricks by assessing the technological, mineral and physical properties of the samples made by using different replacement percentages and relating such properties to their physical behaviour and mineral composition. For this purpose, this research was carried out following industrial procedures and establishing a fairly low cooking temperature (i.e. 900 ºC), with the aim of reducing the energy intensity of fired clay bricks.

2. Materials

2.1. Raw materials

PPR was provided by a factory which produces unbleached softwood "kraft pulp" (*Constitución, Chile*). PPR is produced during screening, barking and chipping processes and it mainly consists of calcium carbonate and cellulose fibers. The residue was directly collected from the debris pile during two weeks and stocked in laboratory. It must be taken into account that dust and/or other elements may be contained by PPR. However, with the aim of assessing a realistic proposal, PPR did not undergo any pre-treatment and only a screening was applied in order to limit PPR particle sizes above 1.5 mm.

Clay matter was collected from a local quarry located in the surroundings of Cauquenes (Chile). At this location, several quarries are being used by local manufacturers and it is also sent to all over Chile for improving other clays (Carrasco and Gajardo, 2000). Clay was stocked in the laboratory and directly used for mixing.

2.2 Samples

Ten samples per series were made by mixing clay and different amounts of PPR. The dosage was referenced to the clay weight in a dry basis. Regarding the addition of water, by increasing the amount of PPR blends required more water for achieving the required workability (Table 1).

INSERT TABLE. Table 1. Codes and dosages of sampled.

The extrusion was carried at 10 MPa and a vacuum pump deaireated the blend. A square die (i.e. 45 × 45 mm) was used and the samples were cut at 160 mm length with the aim of improving the best fitting of specimens for equipment tests. These green test specimens were subject to a drying process which began at 25 ºC and finalized at 105 ºC (increasing rate of 8 ºC h^{-1}). The firing process was developed in a programmable lab furnace (i.e. model LT151150 Meldic®) and the firing curve was set as it shown in Figure 1.

INSERT FIGURE 1. Firing curve

3. Methods

Raw materials were characterized in terms of mineral and chemical composition, particle size distribution and thermal behaviour. Hence, X-ray fluorescence (XRF) (Zetium, PANalytical®) allowed to determine the chemical composition of clay which leads to a better interpretation of the carried out X-ray diffraction (XRD) pattern. This was performed (Empyrean, PANalytical®) to find out the mineralogical composition of fired-, unfired clay and PPR ash. XRD test was developed by using CuKα1 (i.e. wavelength of 1.5418740) in the range of 5 to 80 °2θ (45 kV, 40 mA). The semi-quantitative analysis was based on a comparison with the XRD pattern reported by the International Centre for Diffraction Data and the Rietveld refinement calculation process was applied with the aim of obtaining relatively reliable semi-quantitative results, in accordance with previous authors (Bergmann et al., 1998; Dill, 2016). The raw clay particle size distribution was determined by means of the laser diffraction technique (Mastersizer 3000, Malvern Panalytical®), which is able to measure particle size distributions from 10 nm to 3.5 mm. Thermo gravimetric analysis (TGA), first derivative thermogravimetric analysis (dTGA) and differential temperature analysis (DTA) were determined by means of an STA 6000 (PerkinElmer®) from 25.00 to 900.00 °C at 10.00 °C min^{-1} for both clay and PPR. These last tests provide valuable information regarding the firing process in terms of both energy balance and weight of losses.

Each test specimen was measured (i.e. width, length, and height) and weighted at each stage (i.e. green, dried and fired) in accordance with UNE-EN 772-16:2011. These values lead to determine linear shrinkage and weight losses at each stage, which guide manufacturers for designing die geometries and logistics management. In addition, efflorescence behaviour was observed by following UNE 136029:2019 in order to address the possible effect of a high proportion of potential sulfate content (e.g. $CaSO_4$, K_2SO_4, $MgSO_4$, $FeSO_4$, etc.) or incomplete combustion of the organic matter (e.g. Fe^{++} which forms $FeSO_4$).

Apparent density (AD) and WA were determined by means of the Archimedes method which was performed at 20 ºC for 24 h, according to UNE-EN 772-3:2011 and UNE-EN 772-13:2000.

The apparent porosity (AP) and volumes of open pores and impervious portions were determined by following ASTM C373-88 (2006) and previous researches (Ma et al., 2019).

Due to the high influence of porosity on technological properties of fired clay bricks, BET surface, pore volume and diameter size of pores were measured by means of nitrogen adsorption/desorption cycles at 573 K (Nova1000e, Quantachrome®). In addition, these pores were observed by using scanning electron microscope (SEM) equipment. This device also incorporates an energy dispersive X-ray spectroscopy (EDS) device, working at 20 kV, which allowed to study the chemical composition aggregates contained in the fired matrix.

Thermal characterization was based on the transient method performed with a sensor made of thin double spiral nickel sandwiched between two thin ‘‘Kapton” films and the corresponding measurement equipment (i.e. TPS1500 by HotDisk®) in accordance with ISO 22007-2. In particular, the sensor acts as a plane heat source and a resistance thermometer, which makes it possible to determine the material thermal transport properties, that is, TC, diffusivity (DF) and specific heat capacity (SHC), by analysis of the temperature development in the sensor. The power heat source was set between 80 and 150 W and the time was set between 20 and 80 s. This was carefully controlled in order to prevent the thermal wave from reaching the outer sample boundaries during transient recording. Besides, the characteristic time (i.e. the time taken for the heat from the TPS sensor to reach the outer boundary of the material being tested) was kept between one third and one full characteristic time value.

Mechanical tests involved CS and flexural strength or the so-called modulus of rupture (MOR) which were measured by means of a universal machine (i.e. 15 kN load pistons model 65-L28Z10, Controls ®) in accordance with UNE 67042:1988. CS was determined based on UNE-EN 771-1:2011 standards by means of a universal machine (model c56z00, Controls®). The load was applied at different rates (i.e. from 0.5 to 0.05 N s^{-1}) in order to set the test duration above 60 s according to UNE-EN ISO 7500-1:2016.

The criteria for determining CS regarding brittle material has been widely discussed by previous authors (Iskander and Shrive, 2018) since its real stress–strain curve typically shows two zones (i.e. elastic and plastic zones) rather than one.

The elastic zone shows a linear trend (i.e. forces rapidly rise with an almost constant deformation rate), which ends at the so-called yield stress point. Then a plastic behaviour may be observed. Thus, the forces decrease slightly due to closing of some crack-like voids and then the stress increases again until the so-called ultimate stress value. From this point, the material entirely collapses. Hence, with the aim of showing a more conservative approach, this research reports yield stress values. Finally, samples were tested for determining toxicity, in accordance with the TLCP method 1311 (Ukwatta and Mohajerani, 2017). The carried out values have been compared with the mandatory regulatory levels showed by USEPA (1992) and Spanish Ministerial Order AAA/661/2013 (2013).

4. Results

4.1. Raw Materials

Clays from Central Chile have been studied by previous authors (Pardo et al., 2018). In particular, clays collected from the surrounding areas of this research were characterized by high kaolinite contents and proposed for use in all types of building ceramics products (i.e. floor and wall tiles, structural ceramics, and even refractory bricks).

Used clay was mainly composed by SiO_2 (i.e. 50 % approx.) and Al_2O_3 (i.e. 28 %). It also contained approx. 0.42 % and 9.19 % of CaO and Fe_2O_3 respectively, which led its classification as non-calcareous red clay (i.e. CaO content below 6 or 8% and Fe_2O_3 contents of 5 % or more). The content of fluxing oxides (i.e. 1.74 % of K_2O and 0.33 % of Na_2O) was within the ranges used for bricks manufacturers, which commonly show approx. 1.5 % and 0.5 % for K_2O and Na_2O, respectively. The remained auxiliary fluxing oxides such as MgO and MnO were approx. 1.66 % and 0.10 %, respectively. Other oxides contained by clay were TiO_2, P_2O_5 and SO_3, which represented 1.26, 0.11 and 0.05 %, respectively.

In accordance with these FRX results, the main phases of unfired clay powders were quartz, kaolinite, and minerals from the illite-mica group with minor contents of hematite (Fig. 2a). The semi-quantitative analysis estimated kaolinite, illite, quartz, and hematite contents of approximately 40, 12, 40, and 2%, respectively.

The unidentified peak intensities (approx. 6%) might be explained by the presence of amorphous phases and expectable plagioclase, k-feldspars, dolomite, or halloysite, among others. In addition, it must be mentioned that peaks around 7º (2θ) may correspond to montmorillonite, in accordance with previous analysis from same quarries (Pardo et al., 2018; Carrasco and Gajardo, 2000).

XRD pattern of PPR ash (Fig. 2b) showed calcite and lime, quartz and aluminium oxides as expected (Sutcu and Akkurt, 2009; Sutcu and Akkurt, 2010).

INSERT FIGURE 2. Fig.2. XRD of a) unfired clay and b) PPR ash. A: Albite; Al Aluminium oxides; Il: Illite; Qz: Quartz; L: Lime; kn: Kaolinite; cl: chlorite.

According to EN ISO 14688-1:2018 classification, particle size distribution of used clay showed the absence of gravel and low amount of both fine sand and silt of approx. 8% and 9.5%, respectively. Clay represented over 60 % while coarse sand (i.e. from 2 to 200 um) was approx. 21 % (Fig. 3).

INSERT FIGURE 3. Fig. 3. Particle clay distribution

DTA-TGA analysis of clay (Fig. 4a) showed the removal of the equilibrium moisture followed by an exothermic peak (at approx. 475 ºC), which corresponds to the conversion of α-quartz to ß-quartz (Trindade et al., 2011). Furthermore, a small peak between around 600 ºC may be observed related to the dehydroxylation of kaolinite (Milheiro et al., 2005).

On the other hand, thermal analysis of PPR from DTA-DTG (Fig. 4b) pointed out that PPR burned from 250 ºC and the ash content reached approx. 10 %. The decomposition of carbonates took place between 600 and 700 ºC and the weak endothermic peak from approximately 850 ºC was attributed to the beginning of $CaCO_3$ decarbonization.

INSERT FIGURE 4. Fig. 4. TGA, dTGA and DTA curves for a) clay and b) PPR

4.2. Fired Samples

Weight losses from green to dry state (WG) and from dry to fired state (WF) increased by increasing PPR replacement ratio. In a similar way, drying (DS) and firing shrinkages (FS) were also increased. Therefore, total linear shrinkage (TS) grew from 5.3 % up to 10.8 % (Table 2).

INSERT TABLE 2. Table 2. Weight loss and shrinkages as a function of additive percentage

The addition of PPR led to increase pore size and to reduce total pore volume (i.e. fewer but larger pores) (Fig. 5a). Thus, PPR improved interconnectivity between pores and increased AP (Fig. 5b) while the impervious portion (i.e. closed pores) was slightly reduced by increasing the replacement ratio. Open porosity volume remained almost constant.

INSERT FIGURE 5. Fig. 5. a) AP**, impervious portion and open pore volume. b) Pore size, pore volume and BET surface.**

AD was reduced by adding PPR up to 20 % and WA rose up to 24 % for C17 from 16 % of CRTL (Fig.6a) Regarding mechanical response, CS was highly reduced by the addition of PPR while MOR ranged from 2 to 4 MPa by showing maximum values for C2 and C8 (Fig. 6b).

INSERT FIGURE 6. Fig. 6. a) AD and WA as a function of additive percentage. b) CS and MOR a function of additive percentage

TC (Fig. 7) was reduced from 0.53 W m^{-1} K^{-1} to 0.412 W m^{-1} K^{-1} by increasing the amount of additive from 0 to 17.5 %. Conversely, DF increases with the addition of PPR and led to reduce SHC.

INSERT FIGURE 7. Fig. 7. TC, DF and SHC as a function of additive percentage

Regarding the resulting mineral composition of fired samples, it can be stated that the addition of PPR modifies the XRD pattern of control samples (Fig. 8). As can be seen, new peaks appear that correspond mainly to anorthite and hematite due to the calcium and iron oxides added by PPR and the recrystallization of iron and calcium after the breakdown of the phyllosilicates. Other phases include illite, quartz and Gehlenite. In spite of XRD patterns did not show the background it must be noticed that background is increased by increasing PPR due to the generation of the vitreous phase. The absence of further transformation (e.g. wollastonite, mullite, etc.) has been also confirmed by SEM. SEM-EDS (Fig. 9) analysis taken from three different regions of fired samples at each replacement ratio confirmed the composition to be in the anorthite region of $CaO–Al_2O_3–SiO_2$ ternary system and a rich content of silica with impurities such as iron, potassium, magnesium and sodium. EDS shows the increasing of Ca content by increasing the percentage of PPR. In addition, as shown in SEM images, pores size is enlarged by adding PPR with branching fissures that contributes to reduce CS and increase WA. Porosity is not homogeneous due to the uneven distribution of PPR fibers within the clay matrix.

INSERT FIGURE 8. Fig. 8. XRD pattern as a function of additive percentage. An: Anorthite; Ge: Gehlenite; He: Hematite; Il: Illite; Qz: Quartz.

INSERT FIGURE 9. Fig. 9. SEM of function of PPR percentage a) CTRL, b) C2, c) C8, d) C12 and e) C17

Finally, fired clay samples made by replacing 17.5 % were tested with the aim of determining the levels for toxicity (Table 4), in accordance with the TCLP method.

INSERT TABLE. Table 3. TCLP leaching test results of C17

5. Discussion

5.1. Raw Materials

The content of Fe_2O_3 is quite higher than that typically used by manufacturers (i.e. lower than 9 %) but the amount of total fluxing and auxiliary fluxing agents (i.e. approx. 15 %) is below the considered limits. Fired brick manufacturers commonly limit to 20 % the overall fluxing agents in order to avoid excessive shrinkage (Rehman et al., 2020). In accordance with the chemical composition clay may be classified between illitic-chloritic and reddish layers of kaolinitic clays. Furthermore, the MOR of unfired samples matches with the typical value for kaolinitic clays (i.e. between 1 and 3 MPa) (Garcia-Valles et al., 2019). The particle size distribution also confirms the presence of kaolin (i.e. from 0.5 um to 2 um) and suggest the absence of swelling minerals characterized by particles smaller than 0.5 um (Felhi et al., 2008). Besides, the chemical composition shows a low percentage of alkalis, which is typical of kaolin deposits (i.e. alkalis are commonly washed by rainfall) and it is also corroborated by the XRD pattern performed and similar clays assessed by previous authors in nearby quarries (Meseguer et al., 2011). During firing, crystalline structures of kaolinite and chlorite were affected, but not illite, which is present up to 1000°C.

5.2. Samples

Samples were successfully manufactured regardless the amount of PPR. No bloating effects or efflorescence were observed in any sample, regardless the amount of PPR. However, PPR fibers retain large amounts of water and difficult the flow in the extruder. It has been observed that the mixture of clay and PPR fibers is only produced at high moisture content and the percentage of added water must be geometrically increased for a proportional increasing of plasticity (Table 1). However, as it has been stated by previous authors, the lubricating effect of water became less marked as moisture is increased above 30 or 40 % for kaolinitic clays (Salehi and Salem, 2008). In addition, the increasing of water leads to increase DS, from 4.3 % for CTR to 7.6 % in case of C17. Nevertheless, carried out values are below the threshold of 8

% which is commonly stated by brick manufacturers as the highest percentage, whit the aim of reducing the risk of cracks or fissures during drying. Similar results were carried out by Demir et al. (2005) (i.e. 4.4 % for control samples and 5.2 % for 10 % of PPR replacement). Differences may be explained due to the amount of water for forming since the more plasticity of blends the more drying shrinkage.

During the firing process, the liquid phases and the decomposition of gaseous components lead to compression and expansion of the pores and capillaries, respectively. Porosimetry showed that by increasing PPR addition, pore volume is reduced and pore diameter is increased. Thus, the expansive effect of the decomposition of gaseous components is not prevalent in this case; that is, gaseous components could be released from the internal matrix during the firing process thorough the open pore structure and consequently fired matrix shrinkages rather than expands.

Firing loss shows relatively low values (i.e. approx. 8 %) as might be expected, based on the non-calcareous nature of the clay. For the control series, the initial WF values may be explained by the burning of organic matter and the dehydroxylation of clay minerals. Furthermore, the replacement of clay by PPR leads to an increase in the WF produced by carbonate decomposition and the concomitant CO_2 degassing (Bauluz et al., 2003).

The increasing of porosity reduces AD which shows a proportional decreasing rate. This effect corroborates that open porosity remained quite constant. Thus, Shibib (2015) showed an o_P of 26% and a dry density of 1.7 g cm^{-3} while Sutcu and Akkurt (2010) reported an AD of 39.6% with a correlated density of 1.5 g cm^{-3} when looking for anorthite porous ceramics by adding paper residue. However, regarding the *AD* trend analysis, some discrepancies may be highlighted. For instance, higher rates of decrease were shown by Shibib (i.e. 23% reduction with the addition of 9.6% paper residue) or Demir et al., (2005) (21 and 23% reductions with PPR replacements of 5 and 10%, respectively). Conversely, although Sutcu and Akkurt (2009) set the firing temperature to 1,100 ºC, similar rates of decrease were shown (i.e. 12 and 22% with additions of 10 and 20 % paper residue). Besides, Muñoz et al. (2013) pointed out similar average values regardless the very different clay composition and pressure forming (i.e. density is reduced 20 % for 17 % of addition) (Muñoz et al., 2013). These discrepancies might be explained from the perspective of porosity, but the cited papers did not report such behaviour. Although the specific gravity of PPR contributes to reduce density, the main reason for this lower density is the voids and capillaries induced by the PPR combustion. In addition, the lower temperatureleads to an increase of AP by extending the net of capillaries between pores, as mentioned above. Besides, this effect leads to an increase of WA since; when larger pores are formed, the number of available paths for water increases. This is confirmed by all cited researches (Bories et al., 2014; Sutcu and Akkurt, 2010; Shibib 2015; Sutcu and Akkurt, 2009, Muñoz et al., 2013) which showed close relations between WA and AP and it is also demonstrated in this research. Thus, WA (Fig. 6a) shows same trend than AP which seems to correspond to a geometric behaviour rather than a proportional one. WA rises from approx. 16 %) (i.e. control samples) to 25 % for C17. The WA values are above 20 % for PPR additions beyond 7.5 %, which means that from this percentage the so made bricks should not be used for directly exposed masonries and these walls need to be cladded or rendered.

Regarding the mechanical behaviour, the CS is highly reduced from 11 to 3.2 MPa. In spite of relative variations are similar to those found by previous authors, the absolute values greatly differ among researches. Regardless the firing temperature effect, which obviously influence strength by mineral transformation, the applied pressure for molding and the direction of load application during testing have a major impact on absolute values. On the one hand, it must be noticed that tests were performed perpendicular to the extrusion direction, which led to lower values as stated by Sutcu and Akkurt (2009). These authors revealed differences, for the same samples up to 97 % between the two directions. On the other hand, the applied pressure of the extruder forming samples also represents a key factor. At higher pressure, higher CS but higher energy consumption. For instance bricks formed by pressing at 25 MPa shows CS values above 35 MPa (Muñoz et al., 2013) for similar firing temperature (i.e. 940 ºC). In regards to the influence of pores and strength, some authors have demonstrated that pore volume has a significant impact on the average fracture strength while MOR (Fig. 6b) is highly influenced by the pore size distribution (Wu et al., 2007; Cui et al., 2017), plasticity (Chemani and Chemani, 2012), and pressure formation (Li et al., 2011), among others. In spite of mechanical behaviour is of great importance, nowadays bricks are considered more commonly for insulation rather than structural purposes and, from this point of view, thermal properties are the key factor. TC (Fig. 7) has been reduced from 0.53 W m^{-1} K^{-1} to 0.412 W m^{-1} K^{-1} by increasing the amount of additive from 0 to 17.5 %. Sutcu and Akkurt, (2009) showed TC values of 0.48 W m^{-1} K^{-1} for a 20 % of PPR addition and the same percentage resulted in a TC of 0.469 in Shibib (2015). The AD has been traditionially related to TC. However, it must be noticed that, in spite of AD is reduced from C8 to C12, TC is slightly increased. This can be explained since the porous network is quite reduced due to the effect of fluxing agents. Furthermore, since DF increases with the addition of PPR lower SHC is achieved which implies higher rates of temperature propagation. Hence, so made fired clay bricks should not be considered for passive thermal inertia techniques.

Regarding mineral transformations, PPR certainly modifies the original mineral composition of kaolinitic clay due to the addition of ash to the clay matrix. Thus, the addition of PPR contributes to increase the amount of quartz and hematite as well as calcium structures such as lime, calcite, anorthite and gehlenite. As it has been demonstrated, non-calcareous materials produce high temperature phases such as mullite, while the presence of CaO prevents its formation. Therefore, control sample shows γ-Al_2O_3 which may be considered as a transitory phase of mullite but peak intensity disappears from XRD pattern when PPR is increased (Fig. 8). Trindade et al. (2009) explained that decomposed clay minerals form, in combination with CaO, phases such as gehlenite and anorthite rather than mullite. Besides, in accordance with previous authors (El Ouahabi et al., 2015), by increasing calcium content, the intensities of the main phases of original clay decreases due to the formation of anorthite and gehlenite phases.

Besides, the increasing intensity of the diffraction peaks at 3.2 Å, 3.18 Å, and 4.4 Å for C12 confirms the increasing of anorthite (Gencel, 2015). Although the local effect of an increase in temperature might lead to premature melting of minerals due to the alkali content added by PPR self-combustion (Sutcu et al., 2019), this effect was not highlighted by the XRD and SEM analyses, (Fig. 9). Besides, it must be taken into account that many diffraction effects at high temperature are usually overlapped and some mineral structural parameters may return to the original state, or at least to a close position. Conversely, since the quartz transformation is reversible after cooling, the quartz reflection position can be used as a reference (Miras et al., 2018).

Finally, fired clay samples made by replacing 17.5 % were tested in order to determine toxicity levels (Table 4), in accordance with the TCLP method. The results show that possible heavy metals concentrations passing to the solution are below the regulatory limits, confirming that heavy metals were immobilized in all fired bricks and were not released into the environment (Yaras et al., 2020).

6. Conclusions

The technical feasibility of different percentages of additives has been stated. The use of paper and pulp residues add fluxing agents that show positive effects in term of new phases formed during firing by alkalis and alkali-earths. The increased amount of new formed phases reduces the impact of macroscopic porosity related to the decreasing of mechanical resistance. Studied residues have reduce fired clay bricks density which conduces to lower thermal conductivity. It has also been highlighted that such reduction of density goes hand in hand with an increase of water absorption. The obvious advantages of lightweight fired clay bricks in construction (e.g. lower structural dead load, lower transportation costs, lower thermal conductivity, easier handling, etc.) are limited depending on the end use of the brick, since both compressive strength and water absorption are typically regulated. Thus, water absorption should be limited to a range between 17 and 30% depending on the severity of the climate and the corresponding standard followed (e.g. Indian, Chinese, or US standards, among others). Moreover, the compressive strength should be also set above the regulatory limits (e.g., 5 N mm-2 in Spanish code). These undesired effects limit the amount of residue to a maximum percentage of approximately to 10%. Furthermore, the toxicity of the bricks made in this way has been assessed and, from this point of view, the product is marketable. However, the effect of the proposal in terms of greenhouse gas emissions must be investigated in depth.

Acknowledgements

It must be noticed that this work was supported by the Chilean National Commission on Research and Development (CONICYT) [grant number FONDECYT REGULAR 1180414]. Technical and human support provided by CICT of Universidad de Jaén (UJA, MINECO, Junta de Andalucía, FEDER) and by Centro de Manejo de Residuos y Energía (BIOREN) Universidad de la Frontera (Chile) are gratefully acknowledged. We also acknowledge with gratitude and appreciation the altruistic assistance we enjoyed from Emilio Galán Huertos always we needed.

References

Asquini, L., Furlani, E., Bruckner, S., Maschio, S. (2008) Production and characterization of sintered ceramics from paper mill sludge and glass cullet, Chemosphere, 71(1), pp. 83-89.

ASTM C373-88:2006. Standard Test Method for Water Absorption, Bulk Density, Apparent Porosity, and Apparent Specific Gravity of Fired Whiteware Products.

Bauluz, B., Mayayo, M.J., Fernández-Nieto, C., Cultrone, G., González J.M. (2003) Assessment of technological properties of calcareous and non-calcareous clays used for the brick-making industry of Zaragoza (Spain), Applied Clay Science 24 pp. 121– 126.

Bergmann, J., Friedel, P., Kleeberg, R. (1998) BGMN - A new fundamental parameters based.

Bories, C., Borredon, ME., Vedrenne E., Vilarem, G. (2014) Development of eco-friendly porous fired clay bricks using pore-forming agents: A review, Journal of Environmental Management 143 pp. 186-196.

Carrasco, R., Gajardo, A. (2000) kaolinitic plastic clays in the cauquenes province, Chile. 9th Chilean Congress of Geology, Puerto Varas, Chile, book of expanded abstract, p. 171-175. (Spanish).

Chemani, B., Chemani, H. (2012) Effect of Adding Sawdust on Mechanical-Physical Properties of Ceramic Bricks to Obtain Lightweight Building Material. Mechanical and Mechatronics Engineering 6 (11), art. 11497.

Cui, Z., Huang, Y., Liu, H. (2017) Predicting the mechanical properties of brittle porous materials with various porosity and pore sizes. Journal of the mechanical behavior of biomedical materials 71 pp. 10–22.

Demir, I., Baspınar, M. Serhat, Orhan, M. (2005) Utilization of kraft pulp production residues in clay brick production, Building and Environment 40 pp. 1533–1537.

Dill, H.G. (2016) Kaolin: Soil, rock and ore from the mineral to the magmatic, sedimentary and metamorphic environments, Earth-Science Reviews 161 pp. 16-129.

El Ouahabi, M., Daoudi, L., Hatert, F. et al. (2015) Modified Mineral Phases During Clay Ceramic Firing. Clays Clay Minerals, 63, pp. 404-413.

EN ISO 14688-1:2018 Geotechnical investigation and testing - Identification and classification of soil - Part 1: Identification and description.

Felhi, M., Tlili, A., Gaied, M.E., Montacer, M. (2008) Mineralogical study of kaolinitic clays from Sidi El Bader in the far north of Tunisia, Applied Clay Science, 39(3-4) pp. 208-217.

Garcia-Valles, M., Alfonso, P., Martínez, S., Roca, N. (2019) Mineralogical and Thermal Characterization of Kaolinitic Clays from Terra Alta (Catalonia, Spain), Minerals, 10(2), 142.

Gencel, O. (2015) Characteristics of fired clay bricks with pumice additive, Energy and Buildings, 102, pp. 217-224.

Iskander, M., Shrive, N.(2018) Fracture of brittle and quasi-brittle materials in compression: A review of the current state of knowledge and a different approach, Theoretical and Applied Fracture Mechanics, 97,pp. 250-257.

ISO 22007-2, Plastics-determination of thermal conductivity and thermal diffusivity-part 2: transient plane heat source (hot disc) method, 2008, pp. 1–16.

Kizinievič, O., Kizinievič, V., Malaiškiene, J. (2018) Analysis of the effect of paper sludge on the properties, microstructure and frost resistance of clay bricks, Construction and Building Materials 169 pp. 689–696.

Li, J., Lin, H., Li, J. (2011) Factors that influence the flexural strength of SiC-based porous ceramics used for hot gas filter support. Journal of the European Ceramic Society 31 pp. 825–831.

Ma, B., Su, C.,. Ren, X., Gao, Z., Qian, F., Yang, W., Liu, G., Li, H., Yu, J., Zhu, Q. (2019) Preparation and properties of porous mullite ceramics with high-closed porosity and high strength from fly ash via reaction synthesis process, Journal of Alloys and Compounds, 803, pp. 981-991.

Mandeep, Gupta, G.K., Shukla, P. (2020) Insights into the resources generation from pulp and paper industry wastes: Challenges, perspectives and innovations, Bioresource Technology, 297, pp. 122496.

Meseguer, S., Pardo, F., Jordan, M.M., Sanfeliu, T., González, I. (2011) Ceramic behaviour of some kaolins from Cauquenes Province (VII Region of Maule, Chile) Applied Clay Science 52 pp. 414-418.

Milheiro, F.A.C., Freire, M.N., Silva, A.G.P., Holanda, J.N.F. (2005) Densification behaviour of a red firing Brazilian kaolinitic clay Ceramics International 31, 757-763.

Ministry of Agriculture, Food and Environment of Spain (MAAMA), (2013) Ministerial Order AAA/661/2013, Regulations for waste disposal.

Miras, A., Galán, E., González, I., Romero-Baena, A., Martín, D. (2018) Mineralogical evolution of ceramic clays during heating. An ex/in situ X-ray diffraction method comparison study, Applied Clay Science, 161 pp. 176-183.

Monte, M.C., Fuente, E., Blanco, A., Negro, C. (2009) Waste management from pulp and paper production in the European Union, Waste Management 29 pp. 293–308.

Muñoz V.P., Morales O.M.P., Letelier G.V., Mendívil G.M.A. (2016) Fired clay bricks made by adding wastes: Assessment of the impact on physical, mechanical and thermal properties, Construction and Building Materials 125 pp. 241-252.

Muñoz Velasco, P., Morales Ortíz, M.P., Mendívil Giró, M.A., Muñoz Velasco, L. (2014) Fired clay bricks manufactured by adding wastes as sustainable construction material – A review. Construction and Building Materials 63 pp. 97-107.

Muñoz, P., Juárez, M.C., Morales, M.P., Mendívil, M.A. (2013) Improving the thermal transmittance of single-brick walls built of clay bricks lightened with paper pulp Energy and Buildings 59 pp. 171-180.

Pardo, F., Jordan, M.M., Montero, M.A. (2018) Ceramic behaviour of clays in Central Chile Applied Clay Science 157 pp. 158-164.

Rashid, I., Daraghmeh, N.H., Al Omari, M.M., Chowdhry, B.Z., Leharne, S.A., Hodali, H.A., Badwan, A.A. (2011) Chapter 7 - Magnesium Silicate, Editor(s): Harry G. Brittain, Profiles of Drug Substances, Excipients and Related Methodology, Academic Press, 36, pp. 241-285.

Rehman, M-U., Ahmad, M., Rashid, K. (2020) Influence of fluxing oxides from waste on the production and physico-mechanical properties of fired clay brick: A review, Journal of Building Engineering, 27, 100965.

Ribeiro dos Santos, V., Cabrelon, M.D., de Sousa Trichês, E., Quinteiro, E. (2019) Green liquor dregs and slaker grits residues characterization of a pulp and paper mill for future application on ceramic products, Journal of Cleaner Production, 240, pp. 118220.

Rietveld program for laboratory X-ray sources, it's use in quantitative analysis and structure investigations. Commission of Powder Diffraction, International Union of Crystallography CPD Newsletter 20, pp. 5–8.

Salehi, M., Salem, A. (2008) Effect of moisture content on extrusion process of kaolinitic–illitic clay in manufacturing of ceramic Raschig ring, Journal of Materials Processing Technology, 200 (1-3), pp. 232-237.

Shibib, K.S. (2015) Effects of waste paper usage on thermal and mechanical properties of fired brick, Heat and Mass Transfer, 51 (5) pp.685-69.

Sutcu, M., Akkurt, S. (2009) The use of recycled paper processing residues in making porous brick with reduced thermal conductivity Ceramics International 35 pp. 2625-2631.

Sutcu, M., Akkurt, S. (2010) Utilization of recycled paper processing residues and clay of different sources for the production of porous anorthite ceramics. Journal of the European Ceramic Society 30 pp. 1785-1793.

Sutcu, M., Erdogmus, E., Gencel, O., Gholampour, A., Atan, E., Ozbakkaloglu, T. (2019) Recycling of bottom ash and fly ash wastes in eco-friendly clay brick production, Journal of Cleaner Production, 233, pp. 753-764.

Trindade, M.J., Dias, M.I., Coroado, J., and Rocha, F. (2009) Mineralogical transformations of calcareous-rich clays with firing: A comparative study between calcite and dolomite rich clays from Algarve, Portugal. Applied Clay Science, 42, pp. 345-355.

Trindade, M.J., Dias, M.I., Rocha, F., Prudencio, M.I., Coroado, J. (2011) Bromine volatilization during firing of calcareous and non-calcareous clays: archaeometric implications. Applied Clay Science 53 pp. 489–499.

Ukwatta, A., Mohajerani, A. (2017) Leachate analysis of green and fired-clay bricks incorporated with biosolids. Waste Management, 66 pp. 134-144.

UNE 136029:2019 Clay masonry units. Test for efflorescence

UNE 67042:1988. Piezas cerámicas de arcilla cocida de gran formato. Determinación de la resistencia a flexión. Big Ceramic Pieces of Burned Clay. Determination of the Modulus of Rupture.

UNE-EN 771-1:2011. Specification for masonry units – part 1: clay masonry units.

UNE-EN 772-13:2000 Methods of test for masonry units – part 13: determination of net and gross dry density of masonry units (except for natural stone).

UNE-EN 772-16:2011 Methods of test for masonry units - Part 16: Determination of dimensions

UNE-EN 772-3:2011 Methods of test for masonry units - part 3: Determination of net volume and percentage of voids of clay masonry units by hydrostatic weighing.

UNE-EN ISO 7500-1:2016 Metallic materials - Calibration and verification of static uniaxial testing machines - Part 1: Tension/compression testing machines - Calibration and verification of the force-measuring system (ISO 7500-1:2015).

United States, Environmental Protection Agency (EPA), (1992). Method 1311. Toxicity Characteristics Leaching Procedure.

Vashistha, P., Kumar, V., Singh, S.K., Dutt, D., Tomar, G., Yadav, P. (2019) Valorization of paper mill lime sludge via application in building construction materials: A review, Construction and Building Materials, 211, pp. 371-382.

Vieira, CM.F., Pinheiro, R.M., Sanchez-Rodriguez, R.J., Candido, V.S., Monteiro, S.N. (2016) Clay bricks added with effluent sludge from paper industry: Technical, economical and environmental benefits, Applied Clay Science 132–133 pp. 753–759.

Wu, D., Zhou, J., Li Y. (2007) Mechanical strength of solid catalysts: recent developments and future prospects, AIChE Journal, 53, pp. 2618-2629.

Yaras, A., Sutcu, M., Gencel, O., Erdogmus, E. (2019) Use of carbonation sludge in clay based building materials processing for eco-friendly, lightweight and thermal insulation, Construction and Building Materials, 224, pp. 57-65.

FIGURES

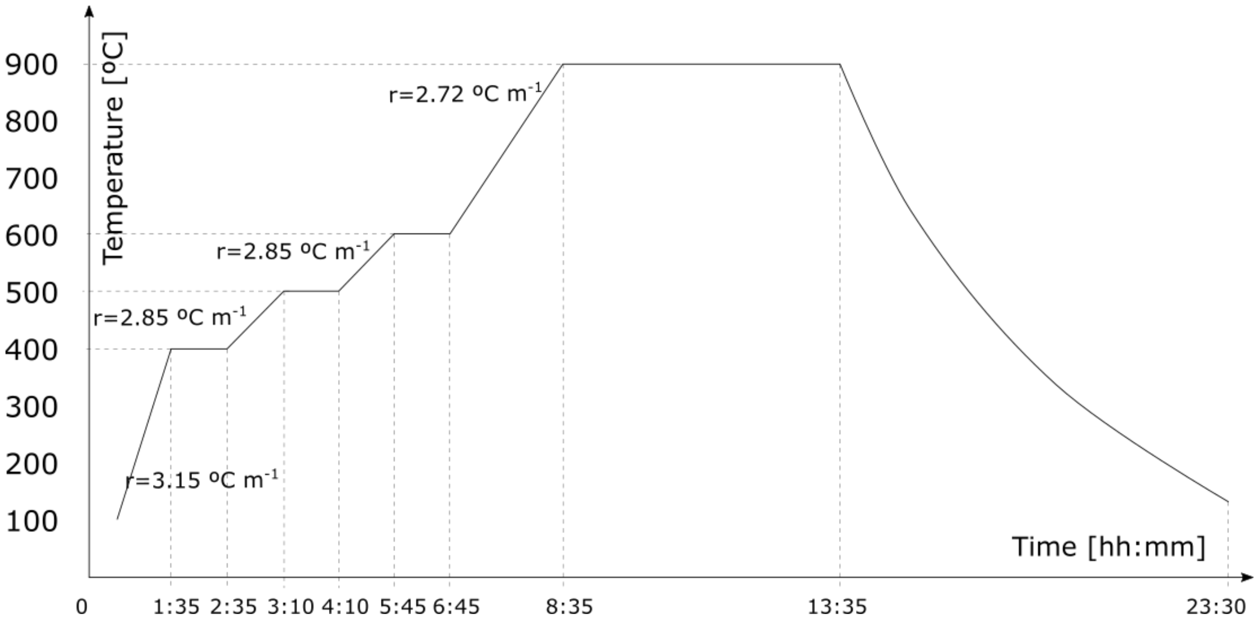

Fig.1. Firing curve

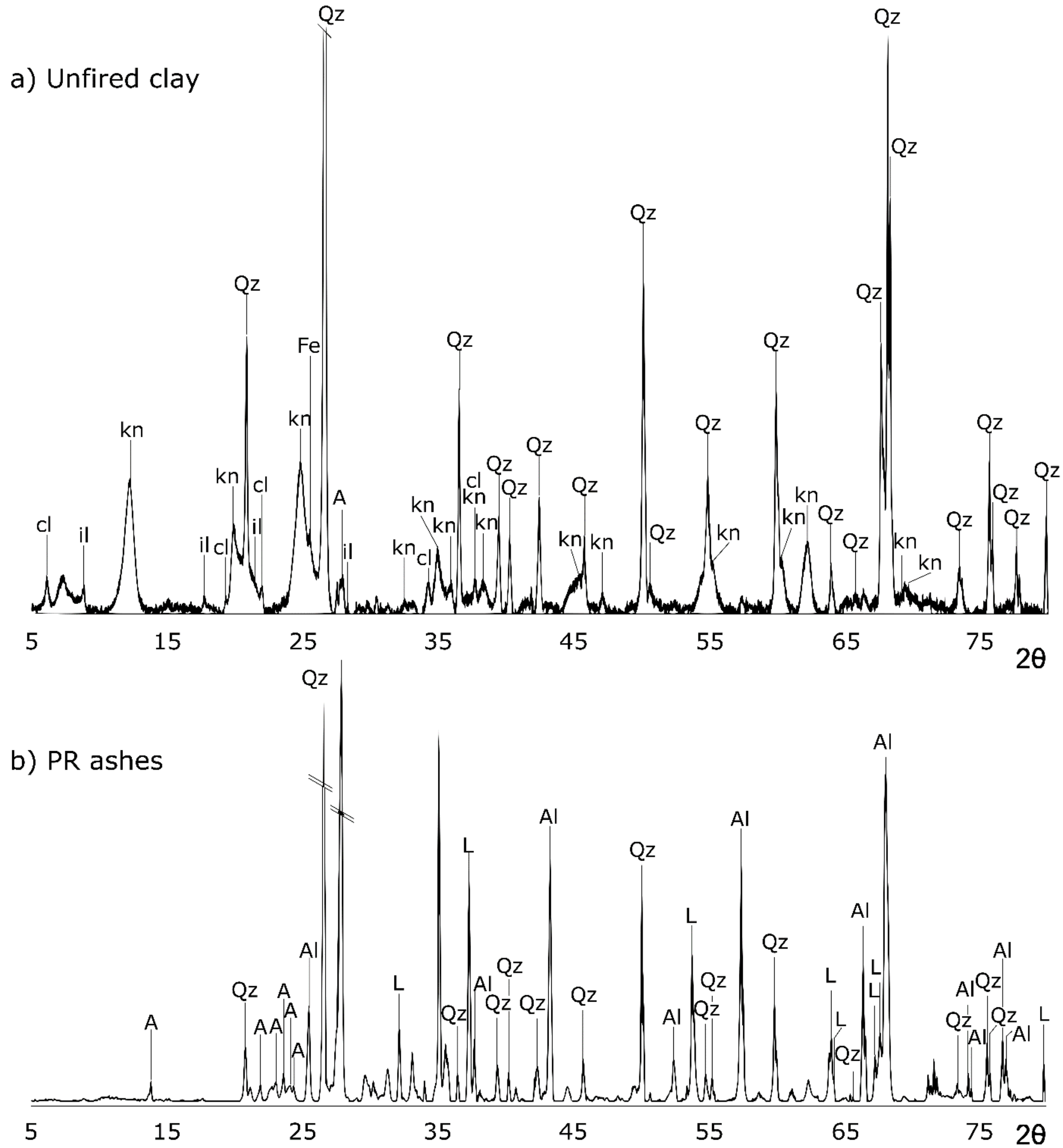

Fig.2. XRD of unfired clay (a) and PPR ash. A: Albite; Al Aluminium oxides; Il: Illite; Qz: Quartz; L: Lime; kn: Kaolinite; cl: chlorite.

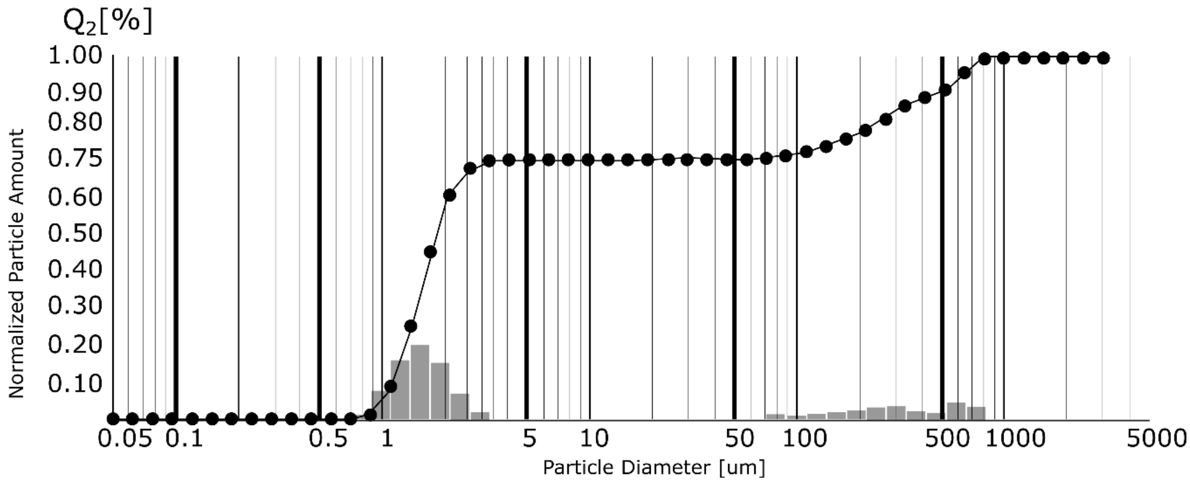

Fig.3. Particle clay distribution

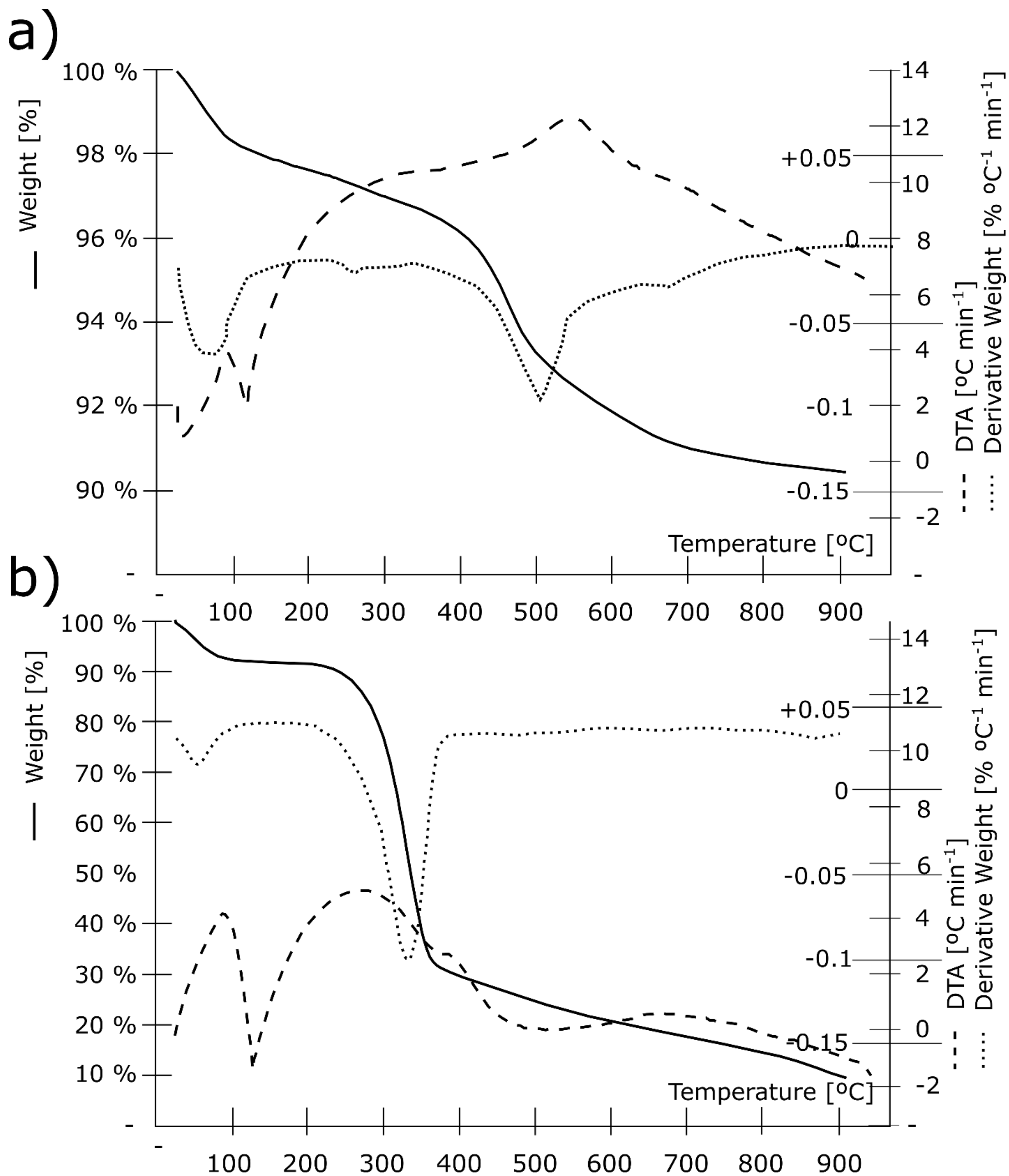

Fig.4. TGA, dTGA and DTA curves for clay (a) and PPR (b)

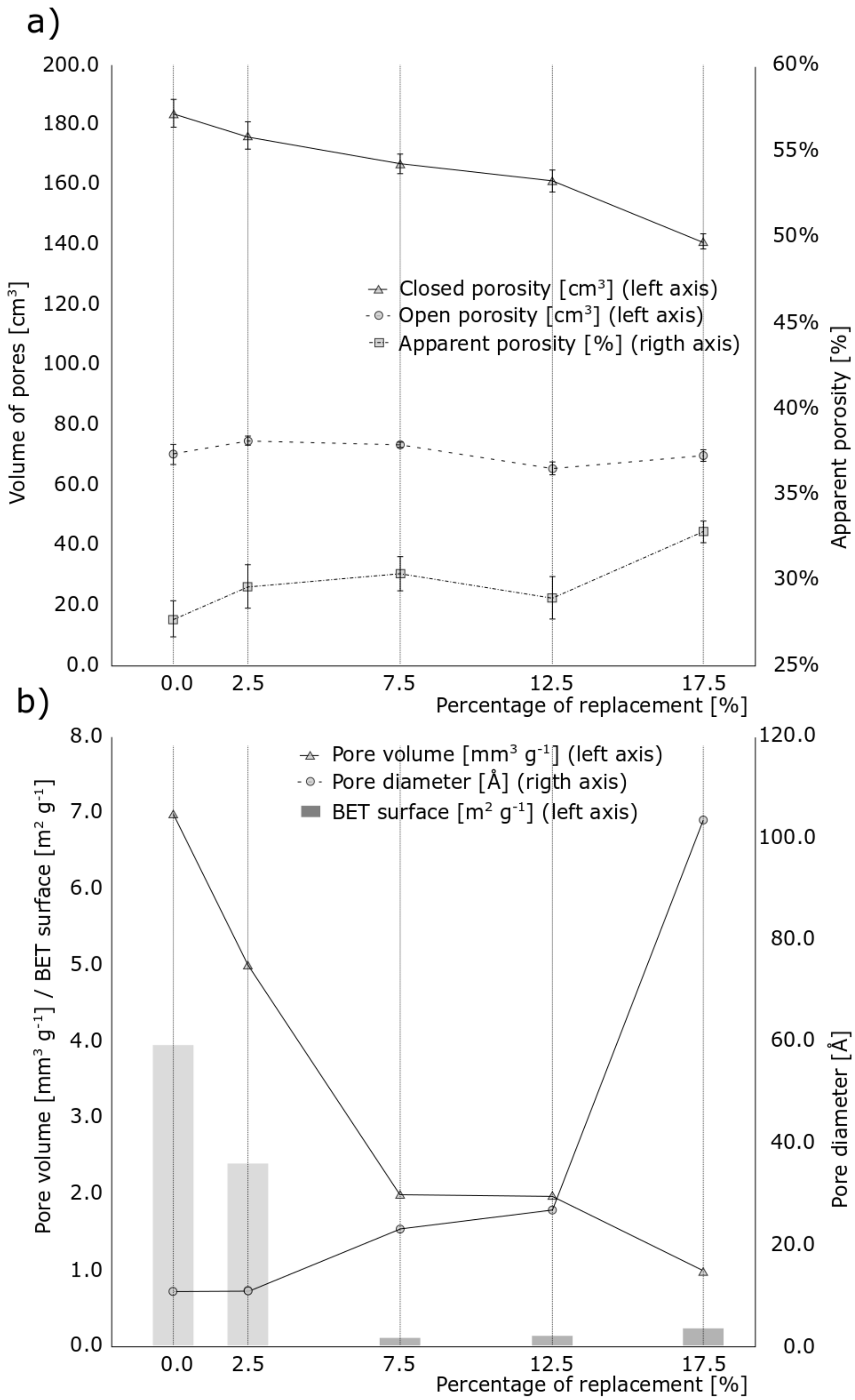

Fig.5. a) AP**, impervious portion and oper pore volume. b) Pore size, pore volume and BET surface.**

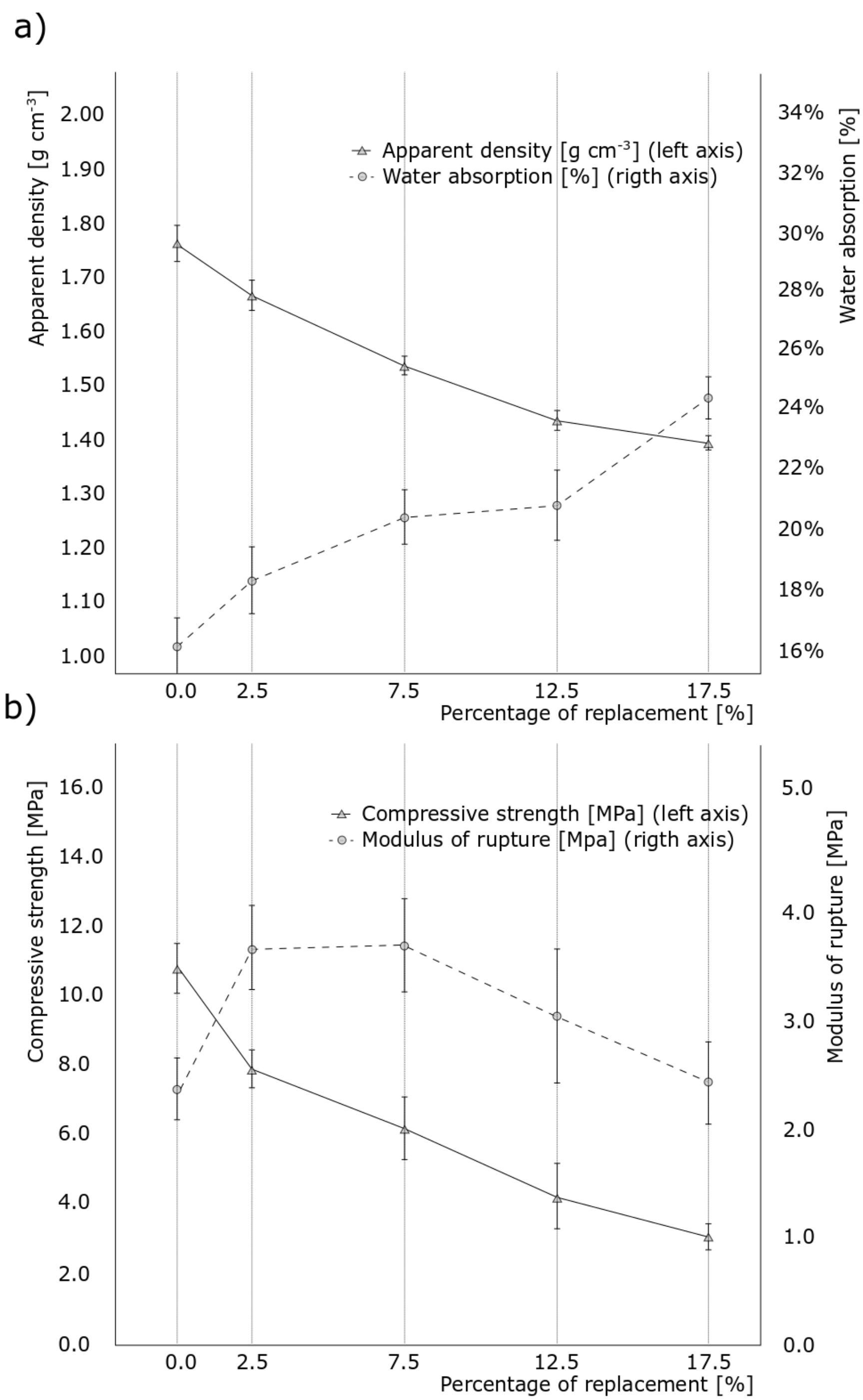

Fig.6. a) AD **and** WA **as a function of additive percentage. b) CS and MOR a function of additive percentage**

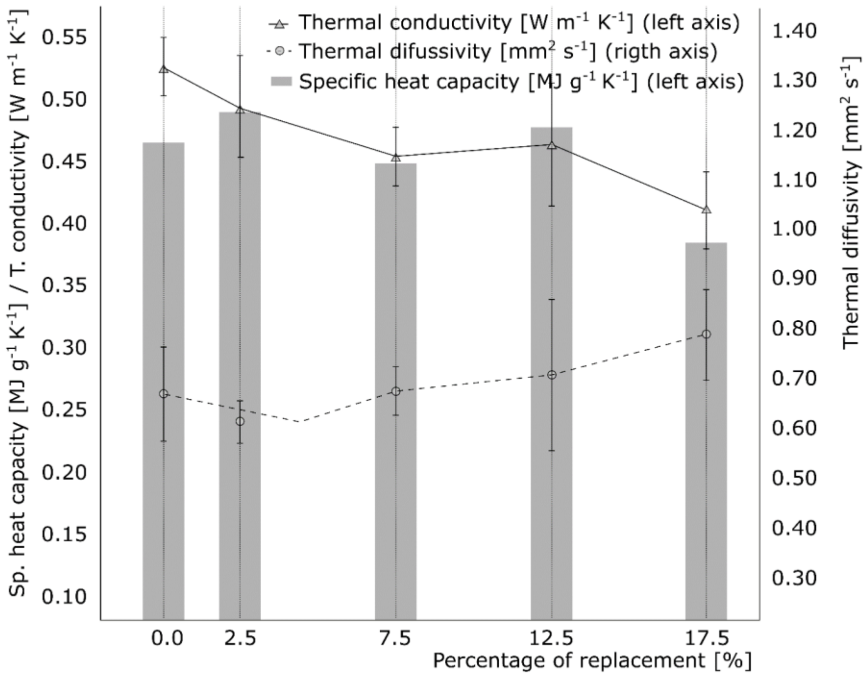

Fig.7. TC, DF and SHC as a function of additive percentage

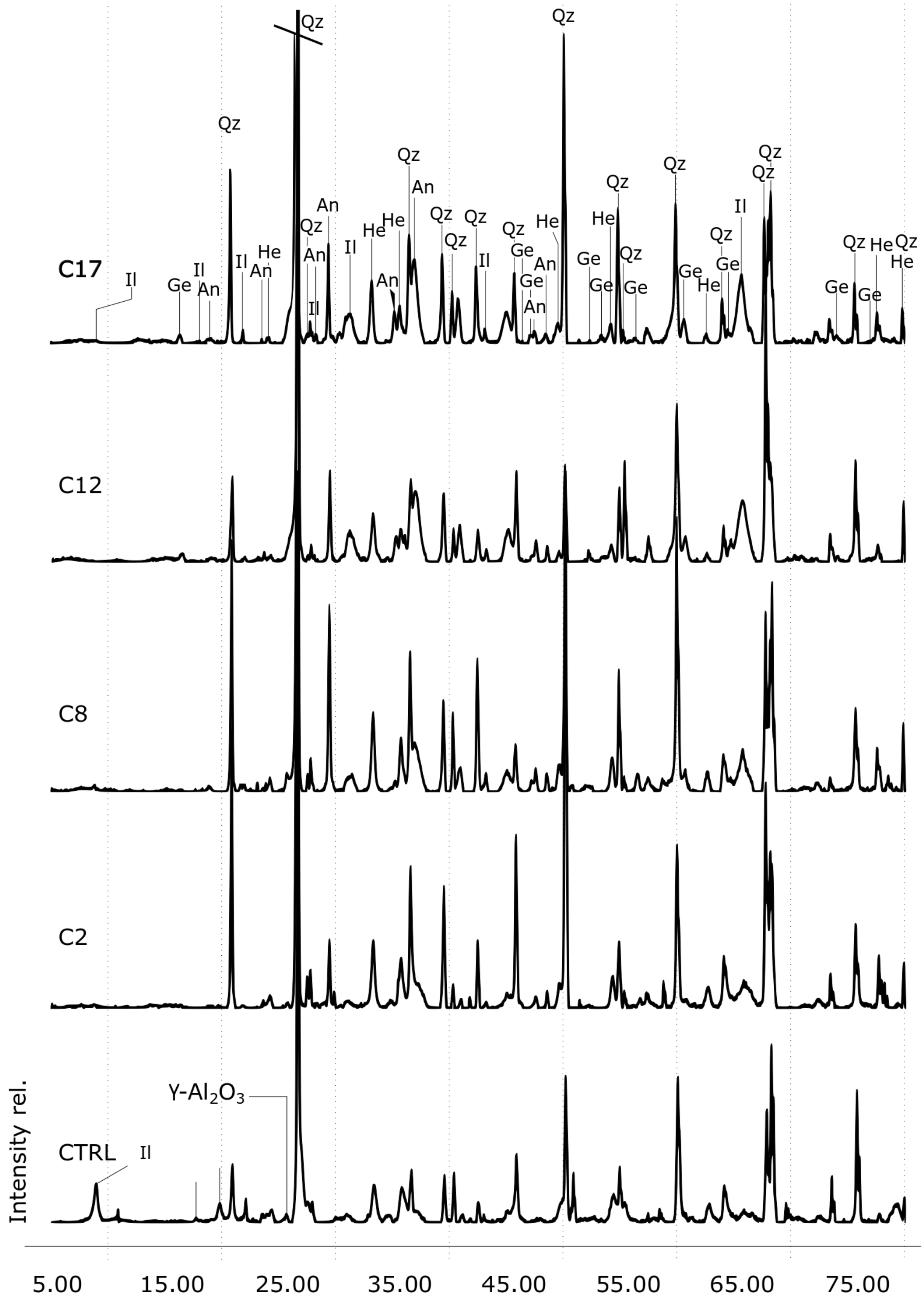

Fig.8. XRD pattern as a function of additive percentage. An: Anorthite; Ge: Gehlenite; He: Hematite; Il: Illite; Qz: Quartz.

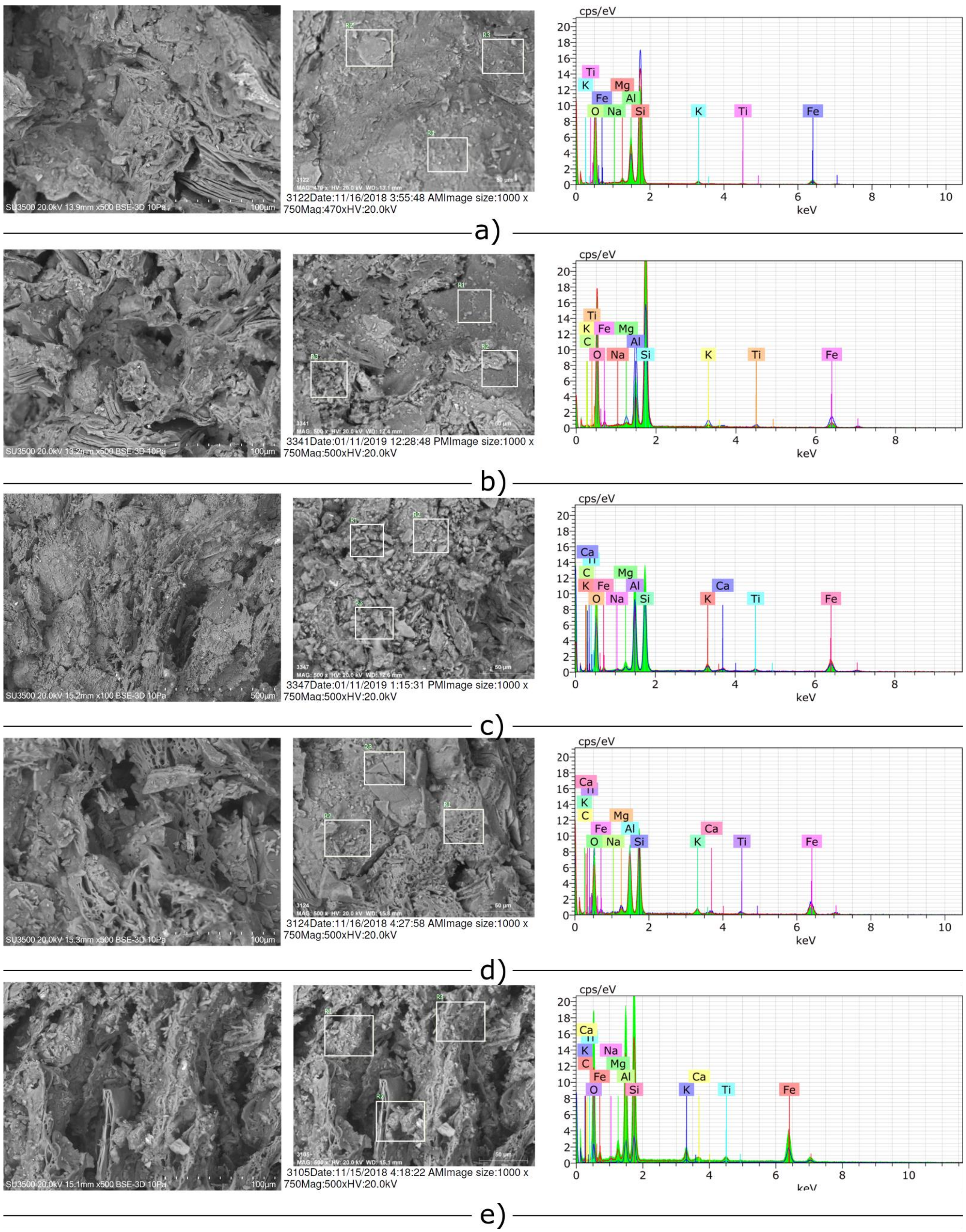

Fig.9. SEM of function of PPR percentage a) CTRL, b) C2, c) C8, d) C12 and e) C17

Table 1. Codes and dosages of sampled.

ID.	Clay [g]	PPR [g]	Water [g]	Clay [%][a]	PPR [%][a]	Water [%][a]	Plasticity index [%][b]
CTRL	7,922.3	–	1,877.7	100	0.0	23.70	22.6 (0.7)
C2	14,755.5	369.8	3,631.8	97.5	2.5	24.01	27.5 (0.5)
C8	12,788.8	959.2	4,298.3	92.5	7.5	31.27	34.5 (0.2)
C12	11,793.4	1,474.2	4,401.9	87.5	12.5	33.18	41.8 (0.3)
C17	11,793.4	2,063.8	4,960.0	82.5	17.5	35.79	47.5 (0.3)

[a] percentage expressed in clay dry basis. [b] Standard deviation (Std. Dev.) is reported between parentheses.

Table 2. Weight loss and shrinkages as a function of additive percentage

ID.	WG [%]*	WF [%]*	TS [%]*	FS [%]*	DS [%]*	MOR**
CTRL	16.8 (0.3)	8.0 (0.1)	5.3 (0.5)	4.3 (0.3)	1.1 (0.5)	1.17 (0.14)
C2	19.7 (0.3)	8.2 (0.1)	6.7 (0.8)	5.5 (0.5)	1.2 (0.7)	2.78 (0.04)
C8	23.0 (0.1)	10.1 (0.1)	7.4 (0.9)	6.3 (0.4)	1.0 (1.1)	2.87 (0.27)
C12	26.0 (0.1)	11.7 (0.1)	9.4 (0.4)	6.9 (0.6)	2.8 (0.5)	2.31 (0.17)
C17	27.7 (0.1)	13.8 (0.1)	10.8 (0.8)	7.6 (0.6)	3.4 (0.5)	1.93 (0.06)

* Standard deviation is reported between parentheses.

** MOR of unfired samples

Table 3. TCLP leaching test results of C17

Element	Units	Value	EPA-TCLP	Spanish Code
Cr	[ug/l]	7,38	5	2,5
Ni	[ug/l]	19,5	-	3
Cu	[ug/l]	15,2	-	30
Zn	[ug/l]	93,7	-	15
As	[ug/l]	12,6	5	300
Se	[ng/l]	<253	106	$2\ 10^{5}$
Ag	[ng/l]	1,16	$5\ 10^{6}$	-
Cd	[ng/l]	53,5	106	$3\ 10^{5}$
Ba	[ug/l]	67,2	105	20
Hg	[ng/l]	<3.6	$2\ 10^{5}$	$3\ 10^{5}$
Pb	[ug/l]	1,89	5	3
Mo	ug/l	10	-	3,5
Sb	ng/l	104	-	$1.5\ 10^{5}$